



## Photoactivable alizarin and eugenol-based materials for antibacterial applications

Christine Eliau, Baptiste Quienne, Sonia Lajnef, Fabienne Peyrot, Régis Moilleron, Samir Abbad Andaloussi, Sylvain Caillol, Davy-Louis Versace

### ► To cite this version:

Christine Eliau, Baptiste Quienne, Sonia Lajnef, Fabienne Peyrot, Régis Moilleron, et al.. Photoactivable alizarin and eugenol-based materials for antibacterial applications. *European Polymer Journal*, 2023, 197, pp.112369. 10.1016/j.eurpolymj.2023.112369 . hal-04188733

**HAL Id: hal-04188733**

**<https://hal.science/hal-04188733>**

Submitted on 26 Aug 2023

**HAL** is a multi-disciplinary open access archive for the deposit and dissemination of scientific research documents, whether they are published or not. The documents may come from teaching and research institutions in France or abroad, or from public or private research centers.

L'archive ouverte pluridisciplinaire **HAL**, est destinée au dépôt et à la diffusion de documents scientifiques de niveau recherche, publiés ou non, émanant des établissements d'enseignement et de recherche français ou étrangers, des laboratoires publics ou privés.

# Photoactivable alizarin and eugenol-based photoinduced materials for antibacterial applications

Christine Elia<sup>a</sup>, Baptiste Quienne<sup>b</sup>, Sonia Lajne<sup>c</sup>, Fabienne Peyrot<sup>c,d</sup>, Régis Moilleron<sup>e</sup>, Samir Abbad Andaloussi<sup>e</sup>, Sylvain Caillol<sup>b</sup>, Davy-Louis Versace<sup>\*a</sup>

<sup>a</sup> Univ. Paris-Est Creteil, CNRS, ICMPE, UMR 7182, 94320 Thiais, France

<sup>b</sup> ICGM, Univ Montpellier, CNRS, ENSCM, Montpellier, France

<sup>c</sup> Université Paris Cité, CNRS, Laboratoire de Chimie et Biochimie Pharmacologiques et Toxicologiques, F-75006 Paris, France

<sup>d</sup> Sorbonne-Université, Institut National Supérieur du Professorat et de l'Éducation (INSPE) de l'Académie de Paris, F-75016 Paris, France.

<sup>e</sup> LEESU, Univ Paris Est Creteil, Ecole des Ponts, , 61 avenue Général de Gaulle, 94010 Créteil Cedex, France.

\* Corresponding author: Prof. Davy-Louis Versace. Email : [davy-louis.versace@u-pec.fr](mailto:davy-louis.versace@u-pec.fr)

## Abstract

We report herein the design of a new visible-light epoxy-based alizarin photosensitizer (AE) of iodonium salt (Iod) for the cationic polymerization (CP) of epoxidized eugenol monomers under visible-light irradiation. The combination of AE and Iod demonstrates highly efficient photoinitiating properties under air. As highlighted by fluorescence, laser flash photolysis (LFP) and electron paramagnetic resonance spin-trapping (ESR ST) experiments, AE acts as an electron donating molecule, and reacts with Iod under light exposure through its excited singlet and triplet states via a photoinduced electron transfer reaction, producing thus protonic acids, H<sup>+</sup>, able to initiate CP. Also, we demonstrate by EPR ST that the addition of diepoxy eugenol monomer may lead to the formation of reactive radical species which may be oxidized by Iod to form cationic species. Thus, new bio-based and photoactivable materials were designed by cationic photopolymerization with the use of alizarin-based photosensitizer and eugenol derived monomers. By tuning the weight proportion of eugenol derived epoxy

monomers (mono- (**EE**) and di-epoxidized (**EdE**) eugenol), we can modulate the thermal and mechanical properties of the resulting materials. The new AE-based materials have demonstrated two interesting properties: first, the presence of EE in the polymer network has considerably decreased the number of colony forming units (CFUs) at the surface of materials whatever the bacterial strains used, and these samples demonstrate photoactivable properties as they produce, under visible-light irradiation, singlet oxygen, a biocide agent against bacteria. Interestingly, the irradiation of the **AE/Iod/EE(50)/EdE(50)** materials lead to a tremendous decrease of the number of *E. coli* and *S. aureus* CFUs at their surface. A reduction by 100% of the bacterial adhesion is observed upon visible-light exposure.

**Keywords.** *Bio-based materials; cationic photopolymerization; antibacterial properties; visible-light irradiation.*

## Introduction

Since the 80's, photopolymerization has gained an incredible interest in many innovative domains *i.e.* in coatings, microelectronics, adhesives, dental applications and more recently, 3D-photoprinting technology [1–3]. Also, photochemical reactions have been widely studied in other valuable fields of innovation such as the synthesis of biomaterials [4], (semi)-interpenetrated networks [5], photoactivable materials [6–9], living/controlled polymerizations [10–14], two-photon polymerizations [6,15–17], spatially controlled polymerizations [18], and so forth.

Light-induced polymerization demonstrated many striking advantages compared to thermal polymerization such as low energy consumption, fast polymerization rates or mild experimental conditions [19,20]. Photopolymerization reactions proceed in few seconds over hours with thermal polymerization, and fewer side reactions (chain transfer reactions) are observed under light-induced reactions in comparison with thermal process [3].

Two different photo-induced mechanisms, *i.e.* free-radical (FRP) and cationic (CP) photopolymerization, have been mainly used in the recent academic and industrial investigations [20]. FRP is limited to olefinic based monomers, which readily react with photoinduced reactive radicals [21]. Although many industrial applications used FRP, oxygen remains the main drawback as it reacts with radicals to produce peroxy radicals which are inefficient to initiate the polymerization under air. Therefore, CP appears as an appealing

alternative to FRP since CP is insensitive to oxygen. In addition, monomers which are prone to CP are known to be less toxic than acrylate or methacrylate ones, and materials resulting from CP show lower shrinkage and residual stress, better abrasion, and chemical resistance than that observed in acrylate (or methacrylate) based materials [19,22,23].

The first example of CP was evidenced by Crivello & Lam in the 1970s by using the photolysis of onium salts under light exposure [24–27]. Different structures of onium salts (OS), including sulfonium [28–31], iodonium [32], pyridinium [33,34], phosphonium [35,36], bismuthium [37], anilinium salts [38] or others [39–41] have been designed and used in academic and industrial applications for the CP of various types of monomers. However, the use of CP raises some issues such as the UV-vis absorption of onium salts or the low thickness of the photoinduced material layers due to the low penetration depth of UV light [42]. Indeed, the spectral sensitivity of OS does not exceed 400 nm and usually leads to CP when exposed to short or mid-UV wavelengths, preventing their use for visible light-induced CP reactions [43]. So, the design of new visible- or IR- light absorbing photosensitizers of OS has become a major issue of concern [25,44]. Different classes of photosensitizers including anthraquinone derivatives, metal carbonyls, organometallic or metallic salt complexes can then be cited [43–47]. Surprisingly, few investigations dealt with the use of natural biobased dyes as photosensitizers of OS [7,9,48,49] and even fewer studies highlight the CP of biobased epoxy monomers. This prompted us to develop first a new visible-light absorbing photosensitizer derived from alizarin, a natural dye extracted from madder roots. The originality of this new dye is the presence of epoxy group on its chemical structure which allows its covalent grafting to the epoxy polymer network during the CP.

Nowadays, the world's natural resources are depleted by the intensive use of non-renewable resources. Stimulated by the global governmental policies towards the use of green sustainable chemistry, the scientific community has focused its attention on the development of new strategies for synthesizing innovative products derived from biomass, which has tremendously grown for decades [50]. To date, biobased polymers such as polysaccharides, polyhydroxyalkanoates, triglyceride derivatives, fatty acids, starch have been widely studied contrary to polyphenols, lignin derivatives, cardanol or eugenol which are under-exploited [51–53]. Fortunately, due to an increasing worldwide production, these families of molecules came to the forefront, and thanks to promising modification methods, the design of new biobased monomers has been recently described [21]. Particularly, the production of epoxy polymers in 2017 reached 3 million tons. The success of the epoxide technology lies in the

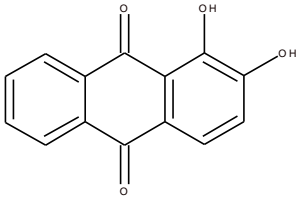
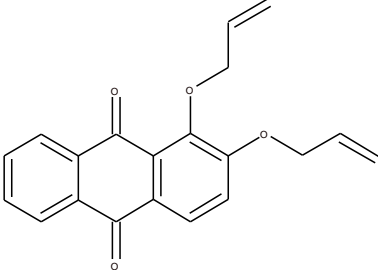
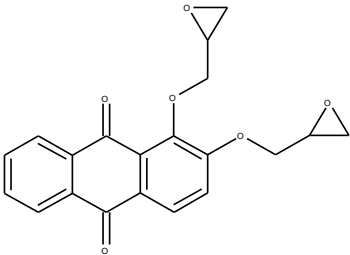
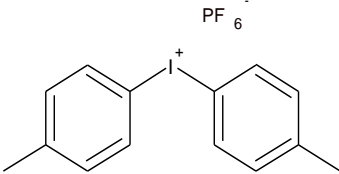
easiness of the modification of the biosourced synthons allowing to tune the mechanical or thermal properties of the resulting materials [19]. The development of new epoxy-based monomers extracted from renewable resources has become a real challenge to avoid for example, the use of hazardous chemicals such as bisphenol A diglycidyl ether, one of the most industrially used epoxy monomers, which is well-known as a reprotoxic R2 substance [54–56]. Biobased synthons such as cardanol, vanillin or eugenol have already been modified to prepare radically photopolymerizable monomers [21] but, and to the best of our knowledge, no investigations concern the CP of epoxy-based eugenol monomers under visible-light irradiation for antibacterial applications. Eugenol [57] is a natural phenolic compound which can be extracted from several plants *i.e.* cinnamon bark, clove buds, turmeric, pepper, oregano or thyme. Eugenol is particularly interesting since it can be a potential alternative to aromatic petro-sourced monomers, and it demonstrated tremendous antibacterial properties.

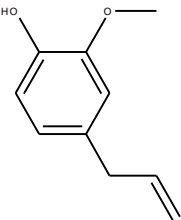
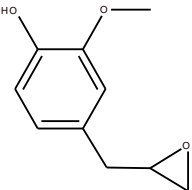
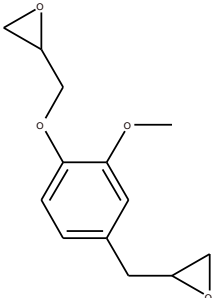
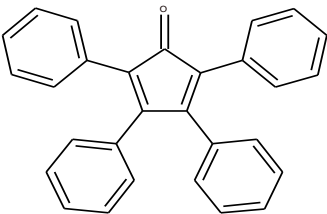
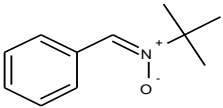
The originality of this study is to design, under visible LED irradiation, new biobased and photoactivable materials from eugenol-based epoxy monomers using a new visible-light absorbing photosensitizer derived from alizarin. In a first part, the photochemical properties of the alizarin-based epoxy photosensitizer will be studied in detail by steady-state photolysis, fluorescence, laser flash photolysis and electron paramagnetic resonance spin-trapping (EPR ST). The cationic photoinitiating performances of this new epoxy-based alizarin photosensitizer when combined with iodonium salt will be also investigated by real time Fourier Transform Infrared spectroscopy (RT-FTIR). In a third part, the swelling index, the gel content, the degradation, and the glass transition temperatures of the different eugenol-based materials will be evaluated, and the photoactivable and the resulting antibacterial properties of the photoinduced materials will be finally tested against *Escherichia coli* and *Staphylococcus aureus* under visible-light exposure.

## Experimental section

**Materials.** Non-modified alizarin (97%, **Aliz**), allyl bromide 99%, potassium carbonate  $\geq 99\%$  ( $K_2CO_3$ ), tetraethylammonium bromide 98% (TEAB), tetrabutylammonium chloride (TBACl), metachloroperbenzoic acid (mCPBA), eugenol, epichlorohydrin, *bis*(4-methylphenyl)iodonium hexafluoro-phosphate 98% (Iod), 3,4-epoxycyclohexylmethyl 3,4-epoxycyclohexanecarboxylate (EPOX), *N-tert- $\alpha$* -phenyl-butyl nitron (PBN), tetraphenylcyclopentadienone (TPCPD) and bromophenol blue sodium salt were purchased from Aldrich, and sodium hydroxide was ordered from Labkem. Solvents used were purchased from Carlo Erba. The structures of the chemicals used in this study are displayed in **Table 1**.

**Table 1.** Chemical structures of the compounds used in this study.

Name	Structure	Role
Alizarin ( <b>Aliz</b> )		Reactant, photosensitizer reference
Alizarin di-allylic derivative ( <b>AA</b> )		Reactive intermediate
Alizarin di-epoxidized derivative ( <b>AE</b> )		Photosensitizer
<b>bis</b> (4-methylphenyl)iodonium hexafluoro-phosphate ( <b>Iod</b> )		Cationic photoinitiator

Eugenol		Reagent
Eugenol mono epoxidized derivative (EE)		Epoxy monomer
Eugenol di-epoxidized derivative (EdE)		Epoxy monomer
Tetraphenylcyclopentadienone (TPCPD)		Reactive oxygen species (ROS) indicator
<i>N</i> -tert-Butyl- $\alpha$ -phenylnitron (PBN)		Spin trap

**NMR spectroscopy.**  $^1\text{H}$  and  $^{13}\text{C}$  NMR spectra were recorded with a Bruker Advance II instrument at 400 MHz and 100 MHz respectively.

**Synthesis of the alizarin allylic derivative (AA).** NaOH (120 mg – 3 mmol – 2 equivalents),  $\text{K}_2\text{CO}_3$  (1.66 g – 12 mmol – 8 equivalents) and tetraethylammonium bromide (TEAB) (96.7 mg – 0.5 mmol – 0.3 equivalent) were ground in a mortar. Alizarin (360.3 mg – 1.5 mmol – 1 equivalent) was added and the resulting solid mixture was transferred to a microwave tube before adding allyl bromide (6 mL– 69.4 mmol – 46 equivalents). In a microwave oven, the tube was heated to 85 °C for 1h30. The blend was transferred in 100 mL of distilled water and extracted with diethyl ether (3x 50 mL). The organic phases

were washed with basic water (NaOH at 1 M) until the aqueous phase was colourless. Indeed, the aqueous phase appears pink when the alcohol groups of alizarin are deprotonated. The resulting organic phases were grouped and dried on anhydrous magnesium sulphate (MgSO<sub>4</sub>) before being filtered and evaporated under vacuum. The obtained solid was purified by silica gel column chromatography with cyclohexane (CyH)/ethyl acetate (AcOEt) eluent (proportion of 90/10 respectively). The final product is the alizarin allylic derivative (AA), an orange powder. Mass yield = 64%. The <sup>1</sup>H, <sup>13</sup>C, Jres, DEPT 135, COSY, HSQC and HMBC NMR spectra are reported in supporting information (Figures S1-7). **<sup>1</sup>H NMR (400 MHz, CDCl<sub>3</sub>) Figure S1.** δ (ppm) 8.25 (m, 2H) **H**<sub>1</sub> – **H**<sub>4</sub>, 8.14 (d, J = 8.6 Hz, 1H) **H**<sub>9</sub>, 7.81 – 7.71 (m, 1H) **H**<sub>2</sub> – **H**<sub>3</sub>, 7.24 (d, J = 1.6 Hz, 1H) **H**<sub>8</sub>, 6.36 – 6.19 (m, 1H) **H**<sub>16</sub>, 6.17 – 6.00 (m, 1H) **H**<sub>12</sub>, 5.51 (d, J = 16.7 Hz, 1H) **H**<sub>17a</sub>, 5.45 (d, J = 16.8 Hz, 1H) **H**<sub>13a</sub>, 5.36 (d, J = 11.0 Hz, 1H) **H**<sub>17b</sub>, 5.29 (d, J = 10.4 Hz, 1H) **H**<sub>13b</sub>, 4.75 – 4.63 (m, 4H) **H**<sub>11</sub> – **H**<sub>15</sub>. **<sup>13</sup>C NMR (100 MHz, CDCl<sub>3</sub>) Figure S2.** δ (ppm) 182.52 **C**<sub>6</sub>, 182.22 **C**<sub>19</sub>, 158.12 **C**<sub>14</sub>, 148.42 **C**<sub>10</sub>, 135.04 **C**<sub>20</sub>, 134.09 **C**<sub>16</sub>, 133.81 **C**<sub>2</sub>, 133.44 **C**<sub>3</sub>, 132.83 **C**<sub>5</sub>, 132.00 **C**<sub>12</sub>, 127.33 **C**<sub>18</sub>, 127.29 **C**<sub>7</sub>, 127.11 **C**<sub>1</sub>, 126.55 **C**<sub>4</sub>, 125.05 **C**<sub>9</sub>, 118.33 **C**<sub>13</sub>, 118.19 **C**<sub>17</sub>, 117.37 **C**<sub>8</sub>, 74.62 **C**<sub>15</sub>, 69.66 **C**<sub>11</sub>.

**Synthesis of the alizarin epoxidized derivative (AE).** Alizarin allylic derivative (AA) (100 mg – 0.31 mmol – 1 equivalent) was dissolved in 5 mL of dichloromethane (DCM). The round flask was equipped with a stirring bar, closed with a septum and degassed with argon flow. In another round flask, metachloroperbenzoic acid (*m*CPBA) (600 mg – 3.5 mmol – 11 equivalents) was dissolved in a minimum of solvent also degassed (4 mL of DCM). The first round flask containing AA in solution was cooled to 0 °C. *m*-CPBA was added dropwise over 1 hour using a syringe and the solution was left to stir for 3 days at room temperature. The colour changed from orange to yellow. The mixture was sequentially washed with a solution of Na<sub>2</sub>SO<sub>3</sub> at 10% (w/v), 100 mL of a saturated solution of NaHCO<sub>3</sub>, and finally with distilled water, in order to remove a maximum of *m*CPBA. The resulting organic phases were grouped and dried on anhydrous MgSO<sub>4</sub> before being filtered and evaporated under vacuum. The obtained solid was purified by silica gel column chromatography with CyH/AcOEt eluent (proportion of 60/40, respectively). The final product is the alizarin epoxidized derivative (AE), a yellow powder. Mass yield = 84%. The <sup>1</sup>H, <sup>13</sup>C, Jres, DEPT 135, COSY, HSQC and HMBC NMR spectra are reported in supporting information (Figures S8-14). **<sup>1</sup>H NMR (400 MHz, Chloroform-d) Figure S8.** δ (ppm) 8.29 – 8.21 (m, 2H) **H**<sub>1</sub> – **H**<sub>4</sub>, 8.16 (d, J = 8.7 Hz, 1H) **H**<sub>9</sub>, 7.82 – 7.68 (m, 2H) **H**<sub>2</sub> – **H**<sub>3</sub>, 7.30 (d, J = 8.6 Hz, 1H) **H**<sub>8</sub>, 4.47 (dd, 1H) **H**<sub>15a</sub>, 4.37 (dd, 1H) **H**<sub>11a</sub>, 4.19 – 4.04 (m, 2H) **H**<sub>15b</sub> – **H**<sub>11b</sub>, 3.61 (m, 1H) **H**<sub>16</sub>, 3.45 (m, 1H) **H**<sub>12</sub>, 2.95 (dd,



1H) **H**<sub>17a</sub>, 2.92 (dd, 1H) **H**<sub>13a</sub>, 2.86 (dd, 1H) **H**<sub>17b</sub>, 2.78 (dd, 1H) **H**<sub>13b</sub>. <sup>13</sup>C NMR (100 MHz, CDCl<sub>3</sub>) **Figure S9**. δ (ppm) 182.47 C<sub>6</sub>, 182.10 C<sub>19</sub>, 157.85 C<sub>14</sub>, 148.33 C<sub>10</sub>, 134.90 C<sub>20</sub>, 133.93 C<sub>2</sub>, 133.60 C<sub>3</sub>, 132.27 C<sub>5</sub>, 127.79 C<sub>18</sub>, 127.77 C<sub>7</sub>, 127.12 C<sub>1</sub>, 126.64 C<sub>4</sub>, 125.34 C<sub>9</sub>, 74.97 C<sub>11</sub>, 69.84 C<sub>15</sub>, 50.63 C<sub>16</sub>, 49.86 C<sub>12</sub>, 44.66 C<sub>17</sub>, 44.40 C<sub>13</sub>.

**Synthesis of mono epoxidized eugenol (EE).** *m*CPBA (77%) (74.86 g, 0.43 mol, 2.4 eq.) was dissolved in 150 mL of ethyl acetate. At 0°C, eugenol (30 g, 0.18 mol, 1 eq.) in 100 mL of ethyl acetate was added dropwise and the reaction was then carried out during 24 h at room temperature. The formed salts were filtered, and the reaction mixture was then washed with NaHCO<sub>3</sub> and brine. The organic layer was then dried with anhydrous MgSO<sub>4</sub> and under vacuum. Flash chromatography was performed in 80/20 cyclohexane/AcOEt to obtain the pure product. Mass yield = 34%. All the EE characterizations by NMR spectra are presented in supporting information (Figures **S15-18**). <sup>1</sup>H NMR (400 MHz, CDCl<sub>3</sub>) **Figure S15** δ (ppm) 6.72 – 6.85 (m, 3H) H<sub>4</sub>-H<sub>6</sub>, 5.53 (s, 1H) H<sub>8</sub>, 3.89 (s, 3H) H<sub>10</sub>, 3.13 (m, 1H) H<sub>12</sub>, 2.78-2.81 (m, 3H) H<sub>13a</sub> and H<sub>11ab</sub>, 2.55 (m, 1H) H<sub>13b</sub>. <sup>13</sup>C NMR (100 MHz, CDCl<sub>3</sub>) **Figure S16**. δ (ppm) 146.5 C<sub>3</sub>, 144.4 C<sub>2</sub>, 129.0 C<sub>7</sub>, 121.7 C<sub>6</sub>, 114.4 C<sub>4</sub>, 111.6 C<sub>5</sub>, 55.9 C<sub>10</sub>, 52.7 C<sub>12</sub>, 46.8 C<sub>13</sub>, 38.4 C<sub>11</sub>.

**Synthesis of di-epoxidized eugenol (EdE).** Monoepoxy-eugenol (11.2 g, 0.062 mol, 1 eq.), epichlorohydrin (58 g, 0.62 mol, 10 eq.) and tetrabutylammonium chloride (1.73 g, 0.006 mol, 0.1 eq.) were reacted at 80 °C for 5 h under stirring. Then, NaOH (7.46 g, 0.19 mol, 3 eq.) was added as a 40 wt% aqueous solution and the reaction was left for 1 h at 80 °C. Once the solution was back to room temperature, the solution was filtered to remove the salt formed after the NaOH addition. 300 mL of CHCl<sub>3</sub> were then added to the solution and washings were performed with H<sub>2</sub>O and then with brine. After the addition of anhydrous MgSO<sub>4</sub> to the organic layer and filtration, the solvent was removed under vacuum and the pure product was obtained. Mass yield = 58%. All the EdE characterizations by NMR spectra are presented in supporting information (Figures **S19-22**). <sup>1</sup>H NMR (400 MHz, CDCl<sub>3</sub>) **Figure S19** δ (ppm) 6.75 – 6.89 (m, 3H) H<sub>4</sub>-H<sub>6</sub>, 3.87 - 4.24 (m, 2H) H<sub>14</sub>, 3.87 (s, 3H) H<sub>10</sub>, 3.37 (m, 1H) H<sub>15</sub>, 3.12 (m, 1H) H<sub>12</sub>, 2.88 (t, 1H) H<sub>16a</sub>, 2.78 – 2.81 (m, 2H) H<sub>13a</sub> and H<sub>11ab</sub>, 2.73 (m, 1H) H<sub>16b</sub>, 2.54 (m, 1H) H<sub>13b</sub>. <sup>13</sup>C NMR (100 MHz, CDCl<sub>3</sub>) **Figure S20**. δ (ppm) 149.6 C<sub>3</sub>, 146.8 C<sub>2</sub>, 131.1 C<sub>7</sub>, 121.1 C<sub>6</sub>, 114.5 C<sub>4</sub>, 112.9 C<sub>5</sub>, 70.4 C<sub>14</sub>, 55.9 C<sub>10</sub>, 52.6 C<sub>12</sub>, 50.3 C<sub>15</sub>, 46.8 C<sub>13</sub>, 44.9 C<sub>16</sub>, 38.3 C<sub>11</sub>.

**UV-Visible spectroscopy.** UV-vis spectra were done on Cary 60 UV-visible spectrometer from Agilent Technologies between 200 nm and 800 nm.

**Irradiation Sources.** Light emitting diodes (LEDs) with emission wavelengths at 385 nm ( $35.3 \text{ mW/cm}^2$ ) and 405 nm ( $101.2 \text{ mW/cm}^2$ ) are provided by Thorlabs.

**Steady-State Photolysis.** AE was dissolved in a DCM solution ( $[\text{AE}] = 4 \times 10^{-4} \text{ M}$ ), and the photosensitive solution was irradiated in a 1 cm-quartz cell under LED@405 nm irradiation. Experiments were also carried out with and without Iod ( $[\text{Iod}] = 5.5 \times 10^{-4} \text{ M}$ ).

**Fluorescence.** Fluorescence spectra were recorded on a FluoroMax+ spectrofluorometer (Horiba Jobin-Yvon) and corrected from the wavelength dependence of the detector sensitivity. The excitation wavelength for both **Aliz** ( $2.66 \times 10^{-6} \text{ M}$ ) and **AE** ( $8.17 \times 10^{-6} \text{ M}$ ) was 380 nm.

**Laser-Flash Photolysis experiments.** Nanosecond laser flash photolysis experiments were performed using a nanosecond Nd:TAG laser (Powerlite 9010, Continuum) set up at 5 Hz and 7-8 ns impulsion time according to a previously described procedure. Samples were irradiated at 355 nm in oxygen-free solution ( $[\text{Aliz}] = 3.67 \times 10^{-4} \text{ M}$  and  $[\text{AE}] = 2.27 \times 10^{-4} \text{ M}$ ) in a 1 cm-width quartz cell at room temperature and under argon atmosphere. The transition absorption spectra of **AE** in ACN and **Aliz** in THF after the addition of Iod at different concentrations were followed at 570 nm.

**Electron paramagnetic resonance (EPR) spin-trapping.** In order to recover the EPR spectra, **AE** was dissolved in dry DCM in the presence of the *N-tert*-butyl- $\alpha$ -phenylnitron spin-trap (PBN) and in presence or not of the co-initiator (Iod) in a 4-mm quartz EPR tube. Oxygen was removed by argon bubbling through the solution for one minute, and the tube was sealed with a septum cap. The spectra were recorded before and after irradiation by the LED@405 nm lamp outside the EPR resonator. EPR measurements were performed using an Eleksys E500 EPR spectrometer (Bruker, Wissembourg, France), operating at X-band (9.8 GHz) and equipped with an SHQ high-sensitivity cavity. Typical settings used were: microwave power, 10 mW; modulation frequency, 100 kHz; modulation amplitude, 0.05 mT; receiver gain, 60 dB; time constant, 10.24 ms; conversion time, 40.96 ms; datapoints, 1024; sweep width, 7 mT; sweep time, 41.94 s. 20 EPR spectra were recorded sequentially at 21°C. Figures present the sum of 5 experimental spectra. Data acquisition and processing were performed using Bruker Xep software. The simulated spectra were calculated with the EasySpin toolbox working on MatLab platform [58].

**Cyclic voltammetry studies.** The oxidation potentials of **Aliz** and **AE** were measured by cyclic voltammetry using a Radiometer Voltalab 6 potentiostat. All the measurements were

carried out in argon-saturated dimethylformamide (DMF) with 0.1 M of tetrabutylammonium hexafluorophosphate ((nBu)<sub>4</sub>NPF<sub>6</sub>) used as supporting electrolyte. The cyclic voltammograms (CVs) were recorded using a three-electrode cell with a glassy carbon electrode as working electrode, a reference saturated calomel electrode and a gold wire electrode as the counter electrode. The free energy changes  $\Delta G$  at the triplet and singlet excited states are evaluated according to the Rehm-Weller equation:  $\Delta G = E_{\text{ox}} - E_{\text{Red}} - E + C$  where  $E_{\text{ox}}$ ,  $E_{\text{Red}}$ ,  $E$ , and  $C$  are the oxidation potential of the electron donor, the reduction potential of the electron acceptor, the excited singlet (or triplet) state energy and the Coulombic term, respectively.  $C$  is usually neglected as experiments are done in polar solvents. Note that  $E_{\text{Red}}$  for Iod = -0.679 V and has been determined in a previous investigation.

**Cationic Photopolymerizations.** The photosensitive formulations (Table 2) were laid down on BaF<sub>2</sub> pellet and irradiated respectively with LEDs@385 and 405 nm under air at room temperature. Kinetics profiles of the epoxy function (790 cm<sup>-1</sup> for EdE and 910 cm<sup>-1</sup> for EE) of the eugenol derived monomers (EE and EdE) with alizarin-based photo-initiating systems were recorded upon irradiation by Real-Time Fourier Transform Infrared spectroscopy (RT-FTIR) on a JASCO FTIR 4700 Instrument. **Aliz** was used as a reference for the photosensibilization of Iod.

**Table 2.** Photosensitive eugenol blend mixtures studied by RT-FTIR at room temperature under air and upon LED irradiation.

Photosensitive formulations	EE proportion (wt%)	EdE proportion (wt%)
<b>AE/Iod/EE(100)</b>	100	0
<b>AE/Iod/EE(75)/EdE(25)</b>	75	25
<b>AE/Iod/EE(50)/EdE(50)</b>	50	50
<b>AE/Iod/EE(25)/EdE(75)</b>	25	75
<b>AE/Iod/EdE(100)</b>	0	100

**Preparation of pellets.** **AE/Iod/EE(100)**, **AE/Iod/EE(75)/EdE(25)**, **AE/Iod/EE(50)/EdE(50)**, **AE/Iod/EE(25)/EdE(75)** and **AE/Iod/EdE(100)** blend mixtures were poured in a round silicon mold (15 mm diameter, 1.3 mm thickness) and irradiated for 10 min on each side under LED@405nm (101.2 mW/cm<sup>2</sup>) exposure.

**Swelling index.** Three samples from the same material, of around 20 mg each, were separately immersed in THF for 24 h. The swelling index (SI) was calculated using Equation 1, where  $m_2$  is the mass of the swollen material and  $m_1$  is the initial mass. Reported swelling index is average values of the three samples.

$$\text{Equation 1} \quad SI = \frac{m_2 - m_1}{m_1} \times 100$$

**Gel content.** Three samples from the same material, of around 20 mg each, were separately immersed in THF for 24 h. The samples were then dried in a ventilated oven at 70 °C for 24 h. The gel content (GC) was calculated using Equation 2, where  $m_3$  is the mass of the dried material and  $m_1$  is the initial mass. Reported gel content is average values of the three samples.

$$\text{Equation 2} \quad GC = \frac{m_3}{m_1} \times 100$$

**Thermal properties.** Materials were synthesized with different proportions of **EE** and **EdE** as described in **Table 2**. Thermogravimetric analyses (TGA) were carried out using TG 209F1 apparatus (Netzsch). Approximately 10 mg of sample were placed in an aluminium crucible and heated from room temperature to 580 °C at a heating rate of 20 °C/min under nitrogen atmosphere (60 mL/min). Differential Scanning Calorimetry (DSC) was performed with a TA Instrument Q25 DSC, following 5 steps in order to compare their thermal properties. The first step was an equilibrate phase at -50°C following by a first heating ramp (up to 150 °C with a rate of 10°C/min), an equilibrate phase at 250°C, a cooling phase (to -50°C with a rate of 10°C/min), an equilibrate phase at -50°C and finally a second heating ramp (to 150 °C with a rate of 10°C/min).

**Release experiments.** Pellets obtained from the **AE/Iod/EE(50)/EdE(50)** and **Aliz/Iod/EE(50)/EdE(50)** formulations were immersed in a small volume of anhydrous THF (5 mL). Samples were continuously agitated on an orbital agitator for 8h, and the solutions were sampled at fixed times to follow the kinetics of release of **Aliz** and **AE** by UV-visible spectroscopy. The percentage of Aliz and AE released from the pellets was determined applying Beer-Lambert's law. Three materials of each system were tested three times.

**Singlet oxygen ( $^1\text{O}_2$ ) detection.** The singlet oxygen ( $^1\text{O}_2$ ) generation of the **AE/Iod/EE(50)/EdE(50)** pellets was investigated in solution using tetraphenylcyclopentadienone (TPCPD) as a common  $^1\text{O}_2$  trap, and under LED@405 nm irradiation. The progress of  $^1\text{O}_2$  generation was followed by the TPCPD oxidation, and by the

subsequent decrease of its absorbance at 505 nm. Pellets were immersed in a methanolic solution of TPCPD ( $6.8 \times 10^{-4}$  M) and irradiated with a LED@405 nm (101.2 mW/cm<sup>2</sup>). At fixed times the decrease of the TPCPD absorbance is monitored by UV-visible spectroscopy. The reference test was carried out by the irradiation of a solution of TPCPD without any materials.

**X-ray photoelectron spectroscopy (XPS).** XPS measurements were performed according to a previous described method [59].

**Antibacterial Assays.** The antibacterial assays were performed on gram-negative and gram-positive bacteria strains *i.e.* *Escherichia coli* and *Staphylococcus aureus*, respectively according to a previous described method [7,9,48]. Briefly, after being incubated in bacterial solutions and after visible-light exposure, we used the counting method to evaluate the number of colony forming units (CFUs) at the surface of the **AE/Iod/EdE(100)** and **AE/Iod/EE(50)/EdE(50)** materials. The idea is to investigate the effect of the alcohol group of eugenol on bacterial properties of the corresponding materials.

## Results and discussion

**Synthesis of eugenol derived monomers.** The eugenol double bond was first epoxidized with *m*-CPBA to give the eugenol mono-epoxidized (EE) monomer. The formation of epoxides was confirmed by <sup>1</sup>H NMR with the disappearance of double bond proton signals at 5.00 - 5.22 ppm and 5.90 ppm, and the subsequent appearance of characteristic epoxy <sup>1</sup>H signals at 2.54 ppm, 2.80 ppm and 3.13 ppm [60]. The glycidylation of EE was then performed using epichlorohydrin to obtain eugenol di-epoxidized (EdE) monomer with a mass yield of 58%. The quantitative glycidylation was confirmed with the disappearance of the phenolic proton at 5.55 ppm and the appearance of signals at 2.76 ppm, 2.89 ppm, 3.38 ppm, 4.03 ppm and 4.22 ppm corresponding to the epoxide protons.

**Synthesis of the alizarin derivatives.** The general procedure for the synthesis of AA and AE is described in **Scheme 1**. AA was synthesized according to a Williamson reaction [61]. The synthesis proceeded in allyl bromide which was used as the reaction solvent, in a sealed vial under microwave irradiation in basic conditions. After 1h30 min of reaction at 85 °C, the reaction was completed, and the crude was purified by flash chromatography on silica gel.



irradiation of AE at 405 nm leads to the appearance of an isobestic point and the formation of new visible-light absorbing species. Noticeably, when **AE** is combined with Iod, the generation of new species is fastened (Figure 1B). It is also interesting to highlight the formation of protonic acids,  $H^+$ , during the photolysis of the **AE**/Iod photoinitiating system under LED@405 nm irradiation according to the bromophenol blue sodium salt method. Indeed, the protonation of bromophenol blue sodium salt results in the decrease of its absorbance at 607 nm (Figure 1C).

To go further in the comprehension of the photochemical process involved in the photosensibilization of Iod by **AE** (or **Aliz**), fluorescence experiments are performed in THF and all the photochemical properties of both **Aliz** and **AE** are summarized in Table 3. Maximum emission wavelength of **AE** is observed at 481 nm and that of **Aliz** at 651 nm. The fluorescence quenching is carried out to learn about the reactivity of the **AE** excited singlet states toward the addition of Iod. The calculation of the free energy change, regarding the possibility of an electron transfer reaction, is also evaluated according to the Rehm-Weller equation (see equation S1 in Supporting Information), and is based on cyclic voltammetry experiments (Figures S24A and S24B for **AE** and **Aliz** respectively). A quenching of fluorescence is evidenced for **AE** upon the addition of different concentrations of Iod (Figure 2), with  $K_{SV}(\text{AE}) = 713 \text{ M}^{-1}$ . On the contrary, no fluorescence quenching is observed with **Aliz** in the same experimental conditions (Figure S25). According to the Rehm-Weller equation which is used to evaluate if an electron transfer reaction from the excited singlet state of **AE** to Iod is possible, the estimated negative value of the free energy ( $\Delta G_s(\text{AE}/\text{Iod}) = -0.742 \text{ eV} < 0$ ) indicates that an electron transfer is allowed. The associated electron transfer quantum yield, deducted from  $\phi_{eT} = K_{SV}[\text{Iod}] / (1 + K_{SV} [\text{Iod}])$ , is very high as  $\phi_{eT} = 0.97$  (with  $[\text{Iod}] = 0.048 \text{ M}$ ) and confirms the highly efficient reaction between the excited singlet state of **AE** and Iod. On the contrary,  $\Delta G_s(\text{Aliz}/\text{Iod})$  is lower than that observed with **AE** and is evaluated at  $+0.098 \text{ eV}$ .

To investigate the reactivity of the excited triplet state of **AE** with Iod, transient absorption experiments using LFP are performed in oxygen free solution in acetonitrile. Two triplet-state absorption bands for **AE** are experimentally observed at 460 and 570 nm (maximum absorption band at 570 nm) (Figure 3A). The triplet state of **AE** decayed with a lifetime of  $5.4 \mu\text{s}$  which is comparable with that observed with AQ ( $6 \mu\text{s}$ ) [65]. As expected, the triplet state of **AE** is efficiently quenched by molecular oxygen: the quenching rate constant ( $k_q \text{ O}_2(\text{AE})$ ) is evaluated at  $1.7 \times 10^8 \text{ M}^{-1} \text{ s}^{-1}$  (Figure 3B) and is consistent with the values

extracted from literature for AQ derivatives [65]. Surprisingly, no excited triplet states are observed for Aliz but a quenching of the triplet state of **AE** is observed: the slope of the regression line of  $1/\tau T$  depending on the concentration of Iod allows to determine a quenching rate constant  $k_q\text{Iod}(\text{AE}) = 7.1 \times 10^8 \text{ M}^{-1} \cdot \text{s}^{-1}$  (**Figure 3C and D**). According to our aforementioned studies, **AE** seems to react with Iod under light exposure through its excited singlet and triplet states.

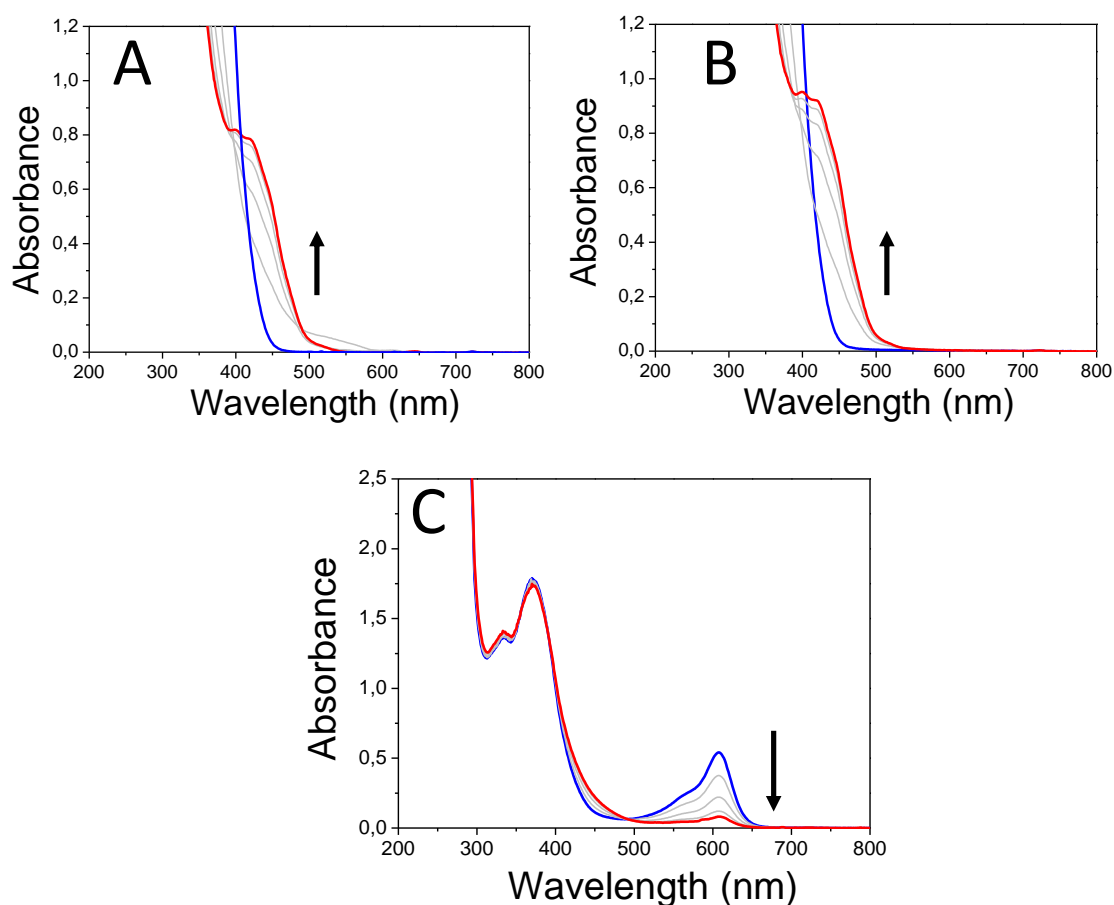


**Figure 1.** Steady-state photolysis of a THF solution of A) **AE**, B) **AE**/Iod after 5 min of LED@405 nm irradiation, and C) **AE**/Iod/ bromophenol blue sodium salt after 4 s upon LED@405 nm exposure and under air.  $[\text{AE}] = 4 \times 10^{-4} \text{ M}$ ,  $[\text{Iod}] = 5.5 \times 10^{-4} \text{ M}$  and  $[\text{bromophenol blue sodium salt}] = 5.3 \times 10^{-6} \text{ M}$ .



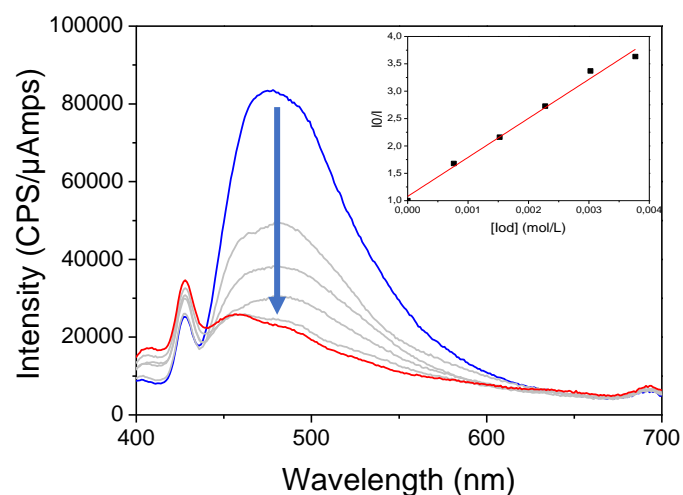


**Figure 2.** Quenching of fluorescence of **AE** ( $[\text{AE}] = 8.17 \times 10^{-6} \text{ M}$ ) with the gradual addition of Iod in THF ( $\lambda_{\text{ex}} = 380 \text{ nm}$ ). Insert: Stern-Volmer plot  $I_0/I = f([\text{Iod}])$  to evaluate the fluorescence quenching constant ( $K_{\text{SV}}$ ).

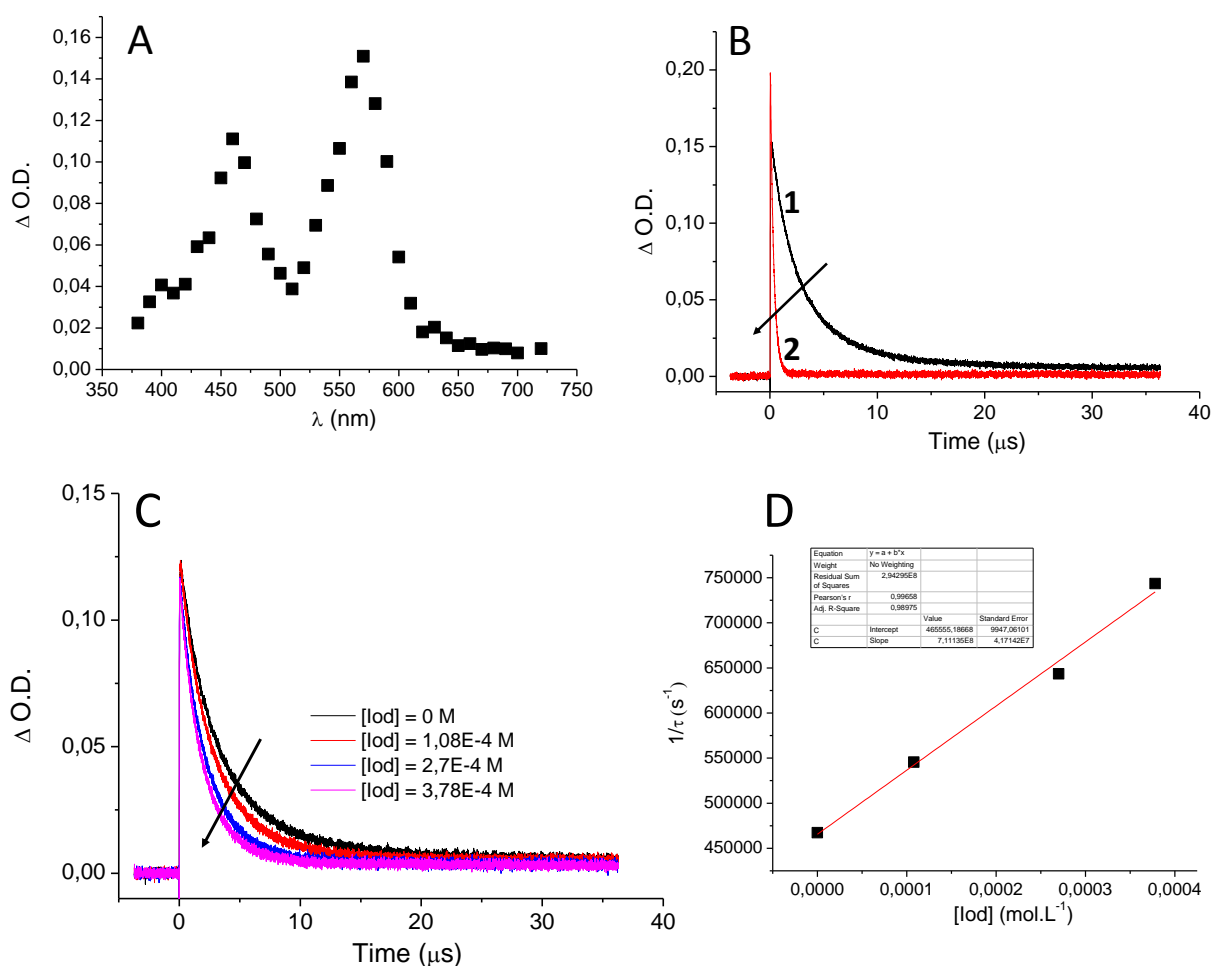


**Figure 3.** A) Transient absorption spectrum of **AE** in an oxygen-free ACN solution after laser pulse ( $\lambda_{\text{ex}} = 355 \text{ nm}$ ), B) Decay traces of **AE** at 570 nm by LFP with and without  $\text{O}_2$ , C) Decay

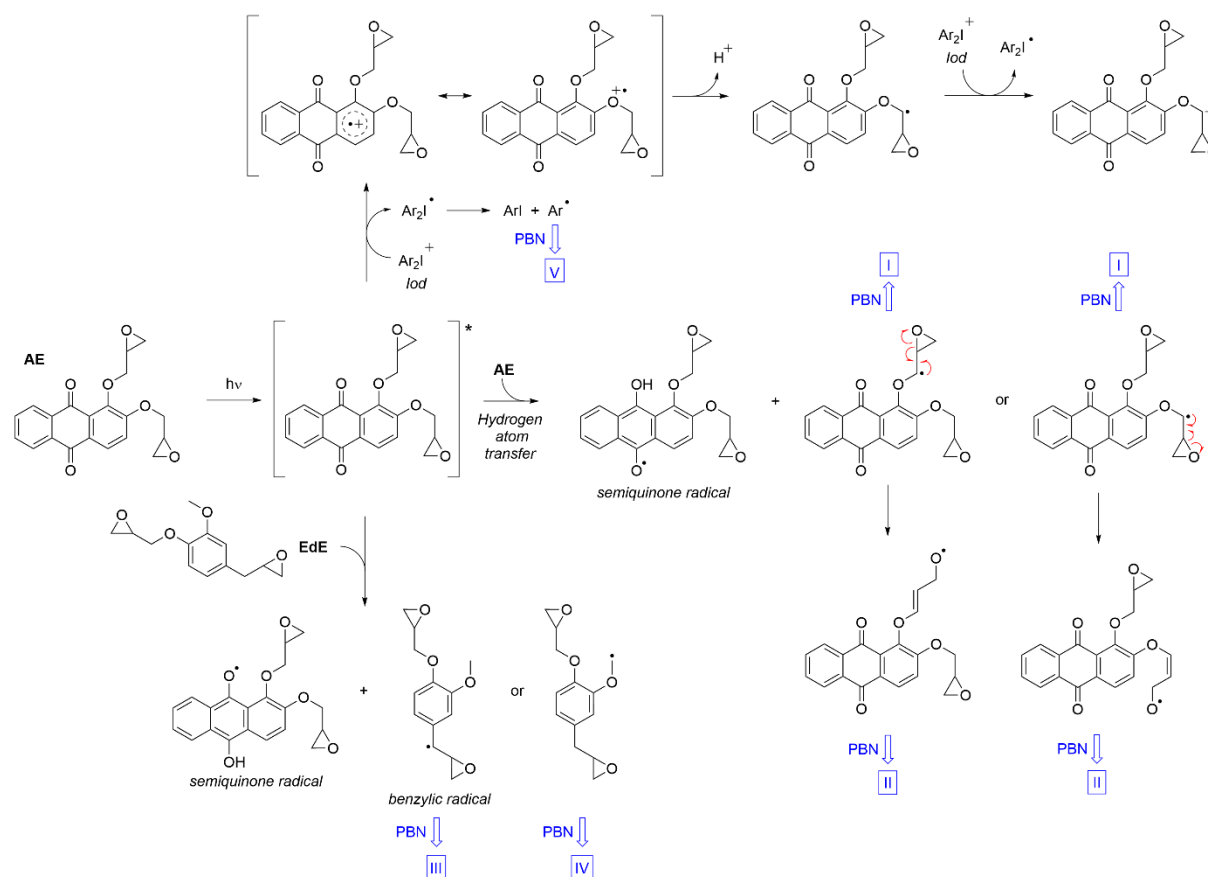
traces of **AE** at 570 nm by LFP with the addition of different concentrations of Iod and C) Stern-Volmer of the corresponding plot.

**Table 3.** Photophysical properties of both photosensitizers (PS) *i.e.* **AE** and **Aliz**.

PS	$\epsilon_{\max}^a$ ( $M^{-1}.cm^{-1}$ )	$\lambda_{abs}^a$ (nm)	$\lambda_{em}^a$ (nm)	$E_{ox}^b$ (V)	$E_S^a$ (eV)	$E_T^c$ (eV)	$K_{SVIod}$ (AE) ( $M^{-1}$ )	$\Delta G_{eT(S)}$ (eV)	$\Delta G_{eT(T)}$ (eV)	$\tau_p$ ( $\mu s$ )	$k_{qIod}$ ( $M^{-1}.s^{-1}$ )
<b>AE</b>	11223	368	481	1.159	2.58	2.18	713	-0.742	-0.342	5.4	$7.1 \times 10^8$
<b>Aliz</b>	5069	431	651	1.319	1.90	-	-	+0.098	-	-	-

<sup>a</sup> In THF, <sup>b</sup> in DMF, <sup>c</sup> in ACN.

EPR ST experiments have been now performed to identify the radical species resulting from the electron transfer reaction between **AE** and Iod. And, for the first time, we also evaluated the influence of the addition of eugenol derived monomer on the nature of the generated radicals when using **AE**/Iod photoinitiating system. All experiments were carried out in DCM under argon atmosphere. The spin-Hamiltonian parameters of the EPR ST signals are provided from simulation experiments and the assignment of the individual paramagnetic radical species is summarized in **Scheme 2**.



**Scheme 2.** Mechanistic approach and proposed assignment of the individual paramagnetic radical species under the irradiation of **AE** based photoinitiating systems.

The LED@405 nm irradiation of AE/PBN/DCM under argon atmosphere results in the immediate formation of two EPR signals (**Figure 4**). The best simulation fit of the experimental spectrum is described as the merge of two signals which are assigned to AE-derived spin adducts with different hyperfine couplings, *i.e.*  $a_N = 1.422$  mT,  $a_H^\beta = 0.296$  mT;  $g = 2.0061$  (species I, **Scheme 2**), which corresponds with PBN-adducts of carbon-centered radicals and  $a_N = 1.351$  mT,  $a_H^\beta = 0.177$  mT;  $g = 2.0063$  (species II, **Scheme 2**), which corresponds with PBN-adducts of oxygen-centered radicals. It seems that an intermolecular hydrogen atom abstraction reaction occurs when **AE** is irradiated leading to semi-quinone radical (unseen) and a carbon-centered radical localized on the  $\alpha$  position of the epoxy group [66] (two isomers are potentially formed with equal probability and cannot be distinguished by spin trapping). Radicals where the unpaired electron is adjacent to an epoxide ring are known to undergo ring rearrangement [67], which could account for the formation of PBN spin adducts of oxygen-centered radicals.

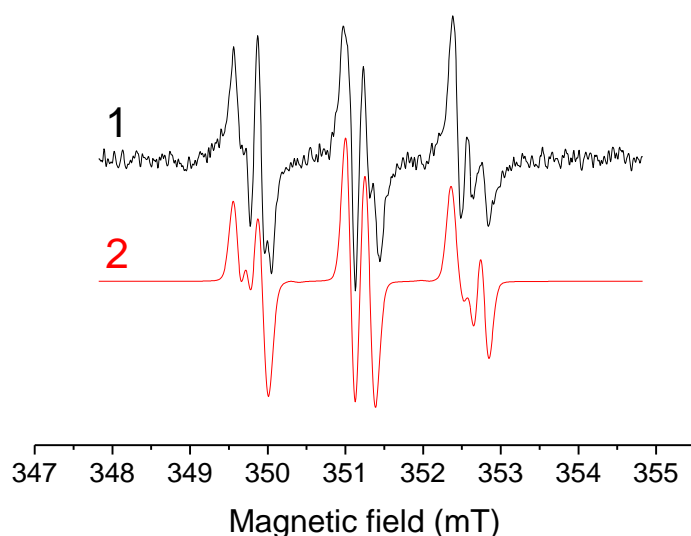


**Figure 4.** Experimental (1) and simulated (2) EPR spectra obtained during 120 s after exposure (LED@405 nm) of **AE**/PBN system. Reactions occur in DCM and under argon atmosphere. Initial concentrations: [**AE**] = 0.028 M; [PBN] = 0.08 M.

The addition of EdE to **AE**/PBN solution leads under LED@405 nm exposure to an EPR spectrum which is interpreted as the superposition of two individual signals (**Figure 5**), *i.e.*

two PBN-adducts of carbon-centered radicals with different hyperfine couplings, *i.e.*  $a_N = 1.507$  mT,  $a_H^\beta = 0.262$  mT;  $g = 2.0061$  (species III, **Scheme 2**), and  $a_N = 1.505$  mT,  $a_H^\beta = 0.308$  mT;  $g = 2.0063$  (species IV, **Scheme 2**). We tentatively assigned these two signals to PBN-adducts of oxymethyl and stabilized benzyl radicals on EdE structure (EdE•), resulting from intermolecular hydrogen transfer between irradiated **AE** and EdE. Indeed, no oxygen-radical spin adduct is observed under these conditions, suggesting that abstraction of hydrogen does not lead to epoxide ring rearrangement [68]. Interestingly, the irradiation **AE**/EdE/Iod/PBN solution at 405 nm results in the immediate formation of a single six-line signal (**Figure 6**) assigned to the PBN-adduct with (4-methyl)phenyl radical (MePh•,  $a_N = 1.462$  mT,  $a_H^\beta = 0.235$  mT;  $g = 2.0061$ , (species V, **Scheme 2**). It is interesting to note that the carbon-centered radicals on EdE structure disappear: these later radicals are likely oxidized by Iod to form cationic reactive species (EdE+) able to promote the CP of epoxy monomer.

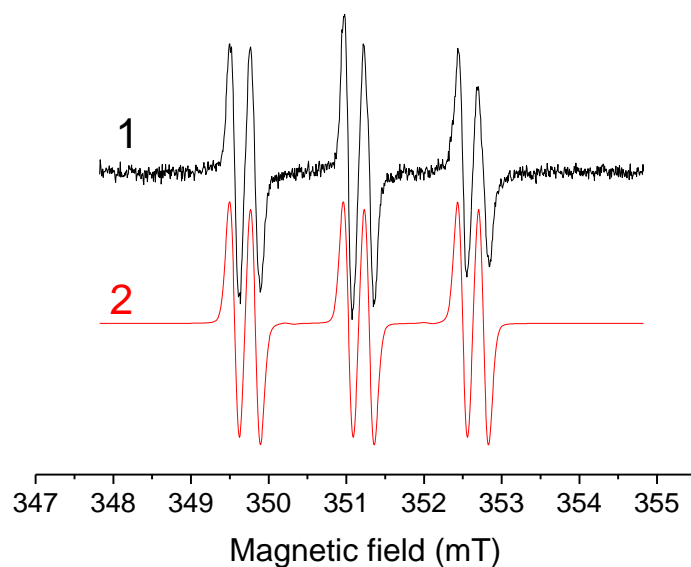


**Figure 5.** Experimental (1) and simulated (2) EPR spectra obtained during 120 s after exposure (LED@405 nm) of **AE**/EdE/PBN system. Reactions occur in DCM and under argon atmosphere. Initial concentrations: [**AE**] = 0.028 M; [EdE] = 0.42 M; [PBN] = 0.08 M.

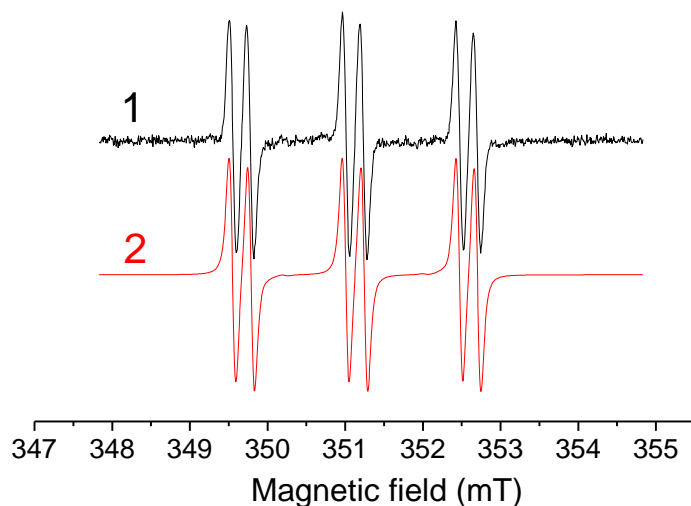


**Figure 6.** Experimental (1) and simulated (2) EPR spectra obtained during 120 s after exposure (LED@405 nm) of **AE**/EdE/Iod/PBN system. Reactions occur in DCM and under argon atmosphere. Initial concentrations: [**AE**] = 0.028 M; [EdE] = 0.42 M; [Iod] = 0.022 M; [PBN] = 0.08 M.

According to fluorescence, LFP and EPR ST results, we can suggest the following mechanisms involved upon the irradiation of the **AE**/Iod/EdE photosensitive formulation: The excitation of **AE** leads concomitantly to a H-abstraction reaction between **AE** and EdE to generate EdE carbon-centered radical (EdE•) and an electron transfer process occurs between the excited singlet and/or triplet states of **AE** and Iod to form methylphenyl radicals and protonic acid, H<sup>+</sup> (photolysis studies). EdE• (species III) is subsequently oxidized by Iod leading to cationic species (EdE<sup>+</sup>). Therefore, both protonic acids and EdE<sup>+</sup> cationic species can be involved in the CP of epoxy monomers (see cationic photopolymerization part). **AE** is subsequently covalently grafted to the epoxy network due to its epoxy groups limiting its release from the materials (see release experiments).

**Cationic photopolymerization studies.** Cationic photopolymerization experiments are carried out using EdE/EE blend mixtures (**Table 2**) with **AE**/Iod as photoinitiating system. Kinetics profiles of the CP of the suggested blend mixtures are followed by RT-FTIR under air and under different irradiation sources *i.e.* LED@385 nm and LED@405 nm (**Figure 7**). **Aliz**/Iod is used as a reference photo-initiating system. The final epoxy conversions after 800 s are reported in Table 4. Interestingly, high final epoxy conversions are obtained after 800 s of irradiation under air whatever the irradiation sources (**Figure 7**). This is likely due to the high absorption properties of **AE** at 385 and 405 nm, and to a lesser extent to the efficient

electron transfer reaction between **AE** and Iod. Interestingly, the CP of EE/EdE blend mixtures with **Aliz**/iod photo-initiating systems leads also to good epoxy conversions (**Figure S26** and **Table 4**): the low  $\Delta G$ s (**Aliz**/Iod) may indicate that an electron transfer reaction between **Aliz** and Iod occurs.

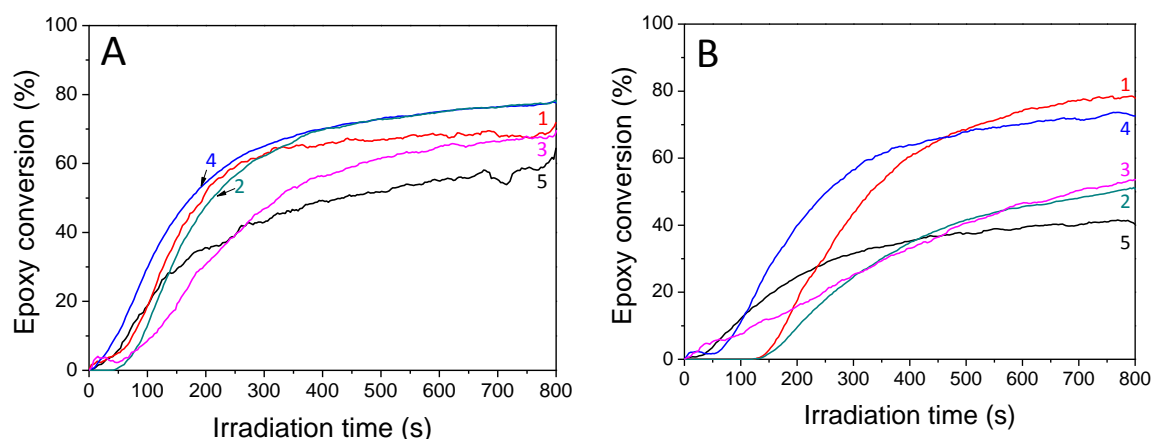


**Figure 7.** Kinetic profiles of the CP of EE/EdE blend mixtures 1) EE 100 wt%, 2) EE 75-EdE 25 wt%, 3) EE 50-EdE 50 wt%, 4) EE 25-EdE 75 wt% and 5) EdE 100 wt%, using **AE**/Iod (0.5%/2% w/w) as photo-initiating system under air and after 800 s of irradiation under A) LED@405 nm and B) LED@385 nm.

**Table 4.** Epoxy conversions of the different EE/EdE blend mixtures determined by IR and using the **AE**/Iod (0.5%/2% w/w) photo-initiating system under air and after 800 s of irradiation under LEDs@385 nm and 405 nm.

Systems studied	Epoxy conversion (%)	
	LED@385 nm	LED@405 nm
<b>AE</b> /Iod/EE(100)	83	72
<b>Aliz</b> /Iod/EE(100)	76	63
<b>AE</b> /Iod/EE(75)/EdE(25)	55	79
<b>Aliz</b> /Iod/EE(75)/EdE(25)	54	75
<b>AE</b> /Iod/EE(50)/EdE(50)	55	70
<b>Aliz</b> /Iod/EE(50)/EdE(50)	73	77
<b>AE</b> /Iod/EE(25)/EdE(75)	72	80

<b>Aliz</b> /Iod/EE(25)/EdE(75)	58	80
<b>AE</b> /Iod/EdE(100)	46	66
<b>Aliz</b> /Iod/EdE(100)	37	61

**Release experiments.** The release experiments (**Figure 8**) have been done with **AE**/Iod/EE(50)/EdE(50) materials because they represent a good compromise between thermal and mechanical properties, and contain sufficient mono epoxidized eugenol (EE) to provide an antibacterial effect. **Aliz**/Iod/EE(50)/EdE(50) materials are used as references. The tack-free materials have been immersed in THF (because of the high solubility of all the separated components in THF), and the percentage of release of **Aliz** (or **AE**) from the corresponding materials is kinetically followed by UV-visible spectroscopy. The kinetics of release are displayed in **Figure 8**. Interestingly, the copolymerization of the epoxy-based alizarin (**AE**) with EE and EdE strongly limits its release from the materials: after 8h, the percentage of **AE** released from the **AE**/Iod/EE(50)/EdE(50) materials (around 10%) is ten times lesser than that observed with **Aliz** (100%) from the **Aliz**/Iod/EE(50)/EdE(50) materials. Surprisingly, 100% of **Aliz** is released from the **Aliz**/Iod/EE(50)/EdE(50) materials in just over 20 min. These results evidence that **AE** is crosslinked to the polymer network during the cationic photopolymerization of eugenol derived monomers.

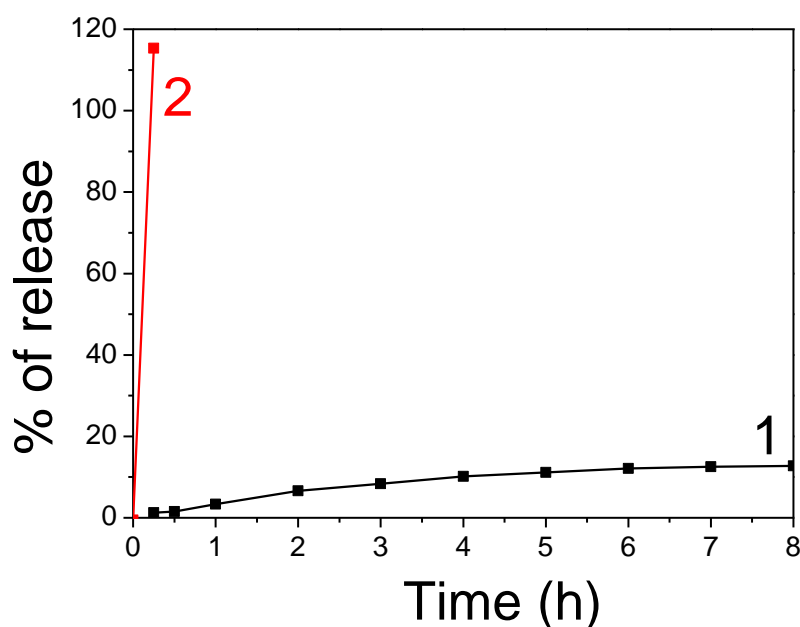


**Figure 8.** Release rate of 1) **AE** from the **AE**/Iod/EE(50)/EdE(50) material and 2) **Aliz** from the **Aliz**/Iod/EE(50)/EdE(50) material after 8h of immersion in THF (average on three materials).

**Material characterization.** The functionalization of alizarin by epoxy group (**AE**) strongly decreases the release of the dye in the medium (**Figure 8**). Therefore, different eugenol-based materials using **AE**/Iod photo-initiating system have been synthesized (**Figure S27**). The glass transition temperature ( $T_g$ ) and the temperature of degradation of the corresponding materials have been determined by differential scanning calorimetry (DSC) and thermogravimetric analyses (TGA), respectively. The swelling index and the gel content of these materials have been also evaluated and all these data are reported in **Table 5**.

The material only composed of EE presents the lower properties. Indeed, since it is monofunctional, it does not allow the formation of a crosslinked network. Therefore, it is fully soluble and presents the lower  $T_g$ . With the addition of EdE to the formulations, the formation of a 3D network is made possible. It results to the increase of the gel contents and  $T_g$  from 18 °C to 52 °C with the increase of EdE concentration. Conversely, swelling index decreases because of the higher crosslinking density induced by the reaction of the difunctional epoxy. On the other hand, the temperature at 5 wt% of degradation ( $T_{5\%}$ ) also increase with EdE concentration (from 195 °C to 285 °C) demonstrating an evolution of the thermal stability with EdE incorporation.

**Table 5.** Swelling index, gel content, degradation and glass transition temperatures of the different eugenol-based materials synthesized after 600 s of LED@405nm irradiation under air for each side.

Name of the materials studied	Swelling index (%)	Gel content (%)	$T_g$ (°C)	Temperature at 5% of degradation $T_{5\%}$ (°C)
<b>AE</b> /Iod/ <b>EE</b> (100)	Soluble	N/A	18	195
<b>AE</b> /Iod/ <b>EE</b> (75)/ <b>EdE</b> (25)	230 ± 73	31 ± 7	24	250
<b>AE</b> /Iod/ <b>EE</b> (50)/ <b>EdE</b> (50)	185 ± 39	85 ± 5	39	275
<b>AE</b> /Iod/ <b>EE</b> (25)/ <b>EdE</b> (75)	75 ± 10	95 ± 3	47	290
<b>AE</b> /Iod/ <b>EdE</b> (100)	23 ± 3	79 ± 2	52	285

**Singlet oxygen detection and antibacterial assays.** To evaluate the capability of the alizarin-based materials (**AE**/Iod/**EE**(50)/**EdE**(50) materials) to produce singlet oxygen ( $^1O_2$ ) once



**AE** is incorporated in the polymer network, TPCPD was used as a singlet oxygen trap. Indeed, when  $^1\text{O}_2$  is produced, TPCPD undergoes a photooxidation reaction resulting in a progressive decrease of its maximal absorption band at 505 nm. The visible-light irradiation of TPCPD solution is carried out with and without **AE**-based pellets and the absorbance of TPCPD solution is followed over time by UV-visible spectroscopy (**Figure 9**). The TPCPD photobleaching is considerably enhanced with the presence of AE-based pellet in solution (**Figure 9B**), thus evidencing the high production of singlet oxygen at the surface of the AE-based pellet. It is noticeable that a slight decrease of the TPCPD absorbance is observed under LED@405 nm irradiation without AE-based pellet (**Figure 9A**). As a result, **AE**-based materials are expected to be photoactivable under visible-light irradiation and should be used as biocide materials to avoid the adhesion of bacteria.

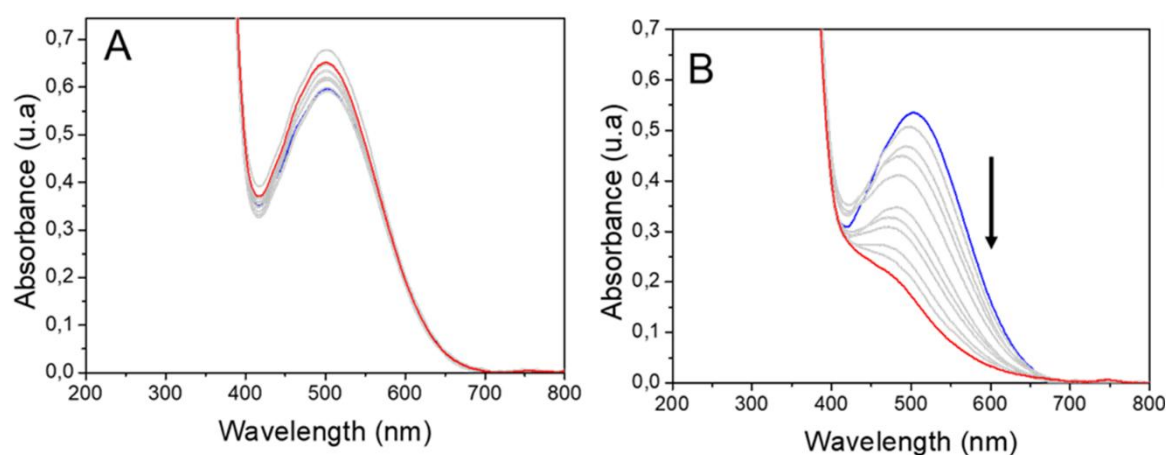


**Figure 9.** UV-vis spectra of a solution of A) TPCPD alone (blank test) and B) TPCPD + (**AE**/Iod/**EE**(50)/**EdE**(50)) pellets in MeOH. UV-vis spectra have been recorded during 20 min upon LED@405 nm exposure.

The ability of the **AE**-based materials to inhibit the adhesion of bacteria on material surface is primarily demonstrated against two bacteria strains *i.e.* *E. coli* and *S. aureus*, and is assessed with and without visible-light activation. Prior to antibacterial tests, samples are incubated one night in each bacteria solution to maximize the adhesion of bacteria on the material surface. After the incubation time, half of the samples are exposed to visible-light, and the other half stay in the dark. Interestingly, only a few colony forming units (CFUs) are observed at the surface of the **AE**/Iod/**EE**(50)/**EdE**(50) materials (**Figure 10B**). The number of CFUs is increasingly low in comparison with bio-based materials that we previously developed. This is likely due to the presence of the phenolic groups of **EE** at the surface of the samples.

Indeed, XPS experiments demonstrated the presence of the C1s signal which is assigned to the phenol group at 286 eV (**Figure S28**). Thus, the antibacterial properties of the **AE**-based materials seem to be due to the disruption of the bacterial membrane after its interaction with the phenol groups. It is noticeable that materials without EE (**AE/Iod/EdE(100)** pellets, **Figure 10A**) show 267- and 9000-times more *E. coli* and *S. aureus* CFUs than those observed on EE-based materials (**AE/Iod/EE(50)/EdE(50)**), confirming the antibacterial effect of EE. Interestingly, the irradiation of the incubated **AE/Iod/EE(50)/EdE(50)** materials leads to a tremendous decrease of the number of CFUs at their surface whatever the bacterial strains used. A reduction by 100% of the bacterial adhesion is observed upon visible-light exposure. Similar results are described for **AE/Iod/EdE** pellets under light activation. These interesting antibacterial results are likely due to the production of  $^1\text{O}_2$  at the surface of the **AE**-based materials upon visible-light activation as above mentioned. These bio-based and photoactivable materials undoubtedly demonstrated their great potentialities for being considered as an alternative for disinfection applications. Note that previous control tests highlighted that light itself has few effects on bacterial proliferation.

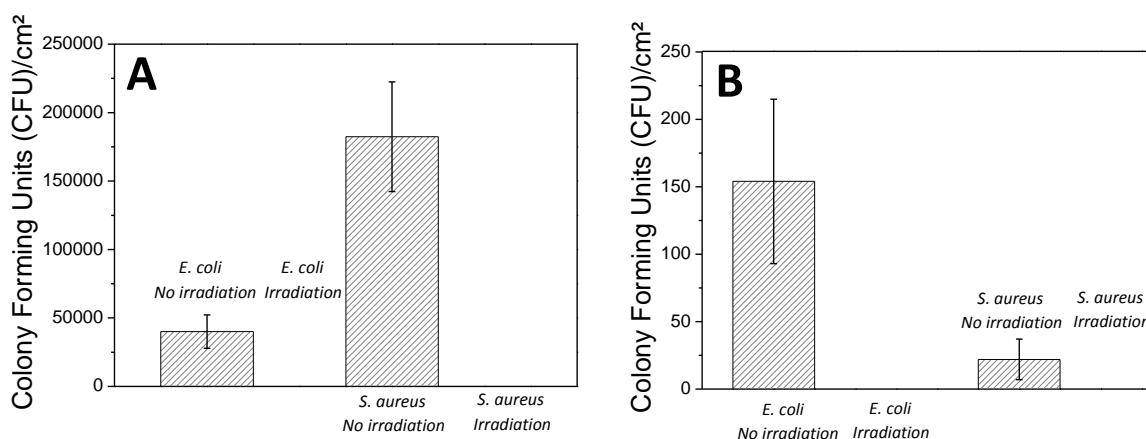


**Figure 10.** Antibacterial properties of the A) **AE/Iod/EdE(100)** and B) **AE/Iod/EE(50)/EdE(50)** materials against *E. coli* and *S. aureus* with and without visible-light exposure.

## Conclusion

This study dealt with the design of a new visible-light epoxy-based alizarin photosensitizer (AE) of iodonium salt (Iod) and the synthesis of new bio-based eugenol derived materials under visible-light irradiation. AE acts as an electron donating molecule and reacts with Iod under LEDs@385 and 405 nm exposure through its excited singlet and triplet states via a photoinduced electron transfer reaction, producing thus protonic acids,  $H^+$ . This new photoinitiating system (AE/Iod) demonstrated very interesting cationic initiating properties under air and light irradiation, using renewable biosourced eugenol derived epoxy monomers (mono- (EE) and di-epoxidized (EdE) eugenol monomers). The cationic photopolymerization experiments using EdE/EE blend mixtures with AE/Iod as photoinitiating system have led to high final epoxy conversion ( $> 70\%$ ). Thus, new bio-based and photoactivable materials have been successfully designed by cationic photopolymerization. By tuning the weight proportion of eugenol derived epoxy monomers (mono- (EE) and di-epoxidized (EdE) eugenol), we demonstrate the capability to modulate the thermal and mechanical properties of the resulting materials. The new AE-based materials have demonstrated two interesting properties: first, the presence of EE in the polymer network has considerably decreased the number of colony forming units (CFUs) at the surface of materials whatever the bacterial strains used, and these samples demonstrate photoactivable properties as they produce, under visible-light irradiation, singlet oxygen, a biocide agent against bacteria. Interestingly, the irradiation of the AE/Iod/EE(50)/EdE(50) materials lead to a tremendous decrease of the number of *E. coli* and *S. aureus* CFUs at their surface. A reduction by 100% of the bacterial adhesion is observed upon visible-light exposure.

## Acknowledgements

Prof. Davy-Louis Versace, Prof. Régis Moilleron and Dr. Samir Abbad Andaloussi would like to thank UPEC, the French Ministry of Higher Education and Scientific Research for financial support.

## Author contributions

**Christine Eliau:** Data analysis, Visualization, Writing-Original draft preparation. **Baptiste Quienne:** Data analysis, Visualization, Writing. **Sonia Lajnef:** Data analysis. **Fabienne Peyrot:** Data analysis, Supervision, Validation, Writing. **Régis Moilleron:** Data analysis.

**Samir Abbad Andaloussi:** Data analysis. **Sylvain Caillol:** Data analysis, Supervision, Writing, Validation. **Davy-Louis Versace:** Conceptualization, Data analysis, Visualization, Writing-Original draft preparation, Writing-Reviewing and Editing, Validation, Supervision.

## References

- [1] J.G. Kloosterboer, Network formation by chain crosslinking photopolymerization and its applications in electronics, in: *Electronic Applications*, Springer-Verlag, Berlin/Heidelberg, 1988: pp. 1–61. <https://doi.org/10.1007/BFb0025902>.
- [2] T.J. Bunning, L.V. Natarajan, V.P. Tondiglia, R.L. Sutherland, Holographic Polymer-Dispersed Liquid Crystals (H-PDLCs), *Annu. Rev. Mater. Sci.* 30 (2000) 83–115. <https://doi.org/10.1146/annurev.matsci.30.1.83>.
- [3] J.-P. Fouassier, J. Lalevée, *Photoinitiators for polymer synthesis: scope, reactivity and efficiency*, Wiley-VCH-Verlag GmbH & Co. KGaA, Weinheim, 2012.
- [4] L. Pierau, D.-L. Versace, Light and Hydrogels: A New Generation of Antimicrobial Materials, *Materials*. 14 (2021) 787. <https://doi.org/10.3390/ma14040787>.
- [5] J. Fouassier, J. Lalevée, Photochemical Production of Interpenetrating Polymer Networks; Simultaneous Initiation of Radical and Cationic Polymerization Reactions, *Polymers*. 6 (2014) 2588–2610. <https://doi.org/10.3390/polym6102588>.
- [6] D.-L. Versace, G. Moran, M. Belqat, A. Spangenberg, R. Méallet-Renault, S. Abbad-Andaloussi, V. Brezová, J.-P. Malval, Highly Virulent Bactericidal Effects of Curcumin-Based  $\mu$ -Cages Fabricated by Two-Photon Polymerization, *ACS Appl. Mater. Interfaces*. 12 (2020) 5050–5057. <https://doi.org/10.1021/acsami.9b18693>.
- [7] P. Sautrot-Ba, J.-P. Malval, M. Weiss-Maurin, J. Paul, A. Blacha-Grzechnik, S. Tomane, P.-E. Mazeran, J. Lalevée, V. Langlois, D.-L. Versace, Paprika, Gallic Acid, and Visible Light: The Green Combination for the Synthesis of Biocide Coatings, *ACS Sustainable Chem. Eng.* 6 (2018) 104–109. <https://doi.org/10.1021/acssuschemeng.7b03723>.
- [8] M. Condat, P.-E. Mazeran, J.-P. Malval, J. Lalevée, E. Renard, S. Abbad Andaloussi, D.-L. Versace, Photoinduced curcumin derivative-coatings with antibacterial properties, *RSC Adv.* 5 (2015) 85214–85224. <https://doi.org/10.1039/C5RA19499G>
- [9] P. Sautrot-Ba, V. Brezová, J.-P. Malval, A. Chiappone, L. Breloy, S. Abbad-Andaloussi, D.-L. Versace, Purpurin derivatives as visible-light photosensitizers for 3D printing and

valuable biological applications, *Polym. Chem.* 12 (2021) 2627–2642. <https://doi.org/10.1039/D1PY00126D>.

[10] J. Xu, S. Shanmugam, H.T. Duong, C. Boyer, Organo-photocatalysts for photoinduced electron transfer-reversible addition–fragmentation chain transfer (PET-RAFT) polymerization, *Polym. Chem.* 6 (2015) 5615–5624. <https://doi.org/10.1039/C4PY01317D>.

[11] S. Shanmugam, J. Xu, C. Boyer, Exploiting Metalloporphyrins for Selective Living Radical Polymerization Tunable over Visible Wavelengths, *J. Am. Chem. Soc.* 137 (2015) 9174–9185. <https://doi.org/10.1021/jacs.5b05274>.

[12] J. Xu, K. Jung, A. Atme, S. Shanmugam, C. Boyer, A Robust and Versatile Photoinduced Living Polymerization of Conjugated and Unconjugated Monomers and Its Oxygen Tolerance, *J. Am. Chem. Soc.* 136 (2014) 5508–5519. <https://doi.org/10.1021/ja501745g>.

[13] A.J. Gormley, J. Yeow, G. Ng, Ó. Conway, C. Boyer, R. Chapman, An Oxygen- Tolerant PET- RAFT Polymerization for Screening Structure–Activity Relationships, *Angew. Chem. Int. Ed.* 57 (2018) 1557–1562. <https://doi.org/10.1002/anie.201711044>.

[14] Y. Guillaneuf, D. Bertin, D. Gigmes, D.-L. Versace, J. Lalevée, J.-P. Fouassier, Toward Nitroxide-Mediated Photopolymerization, *Macromolecules.* 43 (2010) 2204–2212. <https://doi.org/10.1021/ma902774s>.

[15] J.-P. Malval, F. Morlet-Savary, H. Chaumeil, L. Balan, D.-L. Versace, M. Jin, A. Defoin, Photophysical Properties and Two-Photon Polymerization Ability of a Nitroalkoxystilbene Derivative, *J. Phys. Chem. C.* 113 (2009) 20812–20821. <https://doi.org/10.1021/jp9075977>.

[16] N. Hobeika, H. Chaumeil, R. Mhanna, M. Jin, X. Wu, A. Spangenberg, D. Versace, F. Morlet- Savary, J. Malval, Two- Photon Initiating Efficiency of a Ditopic Alkoxynitrostilbene Reacting through a Self- Regenerative Mechanism, *ChemPhysChem.* 21 (2020) 2301–2310. <https://doi.org/10.1002/cphc.202000437>.

[17] M. Jin, J. Xie, J.-P. Malval, A. Spangenberg, O. Soppera, D.-L. Versace, T. Leclerc, H. Pan, D. Wan, H. Pu, P. Baldeck, O. Poizat, S. Knopf, Two-photon lithography in visible and NIR ranges using multibranch-based sensitizers for efficient acid generation, *J. Mater. Chem. C.* 2 (2014) 7201–7215. <https://doi.org/10.1039/C4TC00706A>.

[18] N. Corrigan, F.J. Trujillo, J. Xu, G. Moad, C.J. Hawker, C. Boyer, Divergent Synthesis of Graft and Branched Copolymers through Spatially Controlled Photopolymerization in Flow

- Reactors, Macromolecules. 54 (2021) 3430–3446.  
<https://doi.org/10.1021/acs.macromol.0c02715>.
- [19] L. Pierau, C. Eliau, J. Akimoto, Y. Ito, S. Caillol, D.-L. Versace, Bio-sourced Monomers and Cationic Photopolymerization: The Green combination towards Eco-Friendly and Non-Toxic Materials, *Progr. Polym. Sci.* (2022) 101517.  
<https://doi.org/10.1016/j.progpolymsci.2022.101517>.
- [20] Y. Yagci, S. Jockusch, N.J. Turro, Photoinitiated Polymerization: Advances, Challenges, and Opportunities, *Macromolecules*. 43 (2010) 6245–6260.  
<https://doi.org/10.1021/ma1007545>.
- [21] L. Fertier, H. Koleilat, M. Stemmelen, O. Giani, C. Joly-Duhamel, V. Lapinte, J.-J. Robin, The use of renewable feedstock in UV-curable materials – A new age for polymers and green chemistry, *Progr. Polym. Sci.* 38 (2013) 932–962.  
<https://doi.org/10.1016/j.progpolymsci.2012.12.002>.
- [22] S. Chatani, C.J. Kloxin, C.N. Bowman, The power of light in polymer science: photochemical processes to manipulate polymer formation, structure, and properties, *Polym. Chem.* 5 (2014) 2187–2201. <https://doi.org/10.1039/C3PY01334K>.
- [23] N. Guy, O. Giani, S. Blanquer, J. Pinaud, J.-J. Robin, Photoinduced ring-opening polymerizations, *Progr. Org. Coat.* 153 (2021) 106159.  
<https://doi.org/10.1016/j.porgcoat.2021.106159>.
- [24] J.V. Crivello, J.H.W. Lam, Diaryliodonium Salts. A New Class of Photoinitiators for Cationic Polymerization, *Macromolecules*. 10 (1977) 1307–1315.  
<https://doi.org/10.1021/ma60060a028>.
- [25] J.V. Crivello, J.H.W. Lam, Dye-sensitized photoinitiated cationic polymerization, *J. Polym. Sci. Polym. Chem. Ed.* 16 (1978) 2441–2451.  
<https://doi.org/10.1002/pol.1978.170161004>.
- [26] J.V. Crivello, The discovery and development of onium salt cationic photoinitiators, *J. Polym. Sci. A Polym. Chem.* 37 (1999) 4241–4254. [https://doi.org/10.1002/\(SICI\)1099-0518\(19991201\)37:23<4241::AID-POLA1>3.0.CO;2-R](https://doi.org/10.1002/(SICI)1099-0518(19991201)37:23<4241::AID-POLA1>3.0.CO;2-R).
- [27] J.V. Crivello, J.H.W. Lam, Photoinitiated cationic polymerization with triarylsulfonium salts, *J. Polym. Sci. Polym. Chem. Ed.* 17 (1979) 977–999.  
<https://doi.org/10.1002/pol.1979.170170405>.
- [28] J.V. Crivello, J.H.W. Lam, Complex triarylsulfonium salt photoinitiators. I. The identification, characterization, and syntheses of a new class of triarylsulfonium salt

photoinitiators, J. Polym. Sci. Polym. Chem. Ed. 18 (1980) 2677–2695. <https://doi.org/10.1002/pol.1980.170180825>.

[29] S. Denizligil, Y. Yagci, C. McArdle, Photochemically and thermally induced radical promoted cationic polymerization using an allylic sulfonium salt, Polymer. 36 (1995) 3093–3098. [https://doi.org/10.1016/0032-3861\(95\)97870-L](https://doi.org/10.1016/0032-3861(95)97870-L).

[30] J.V. Crivello, S. Kong, Synthesis and Characterization of Second-Generation Dialkylphenacylsulfonium Salt Photoinitiators, Macromolecules. 33 (2000) 825–832. <https://doi.org/10.1021/ma991661n>.

[31] J.V. Crivello, S. Kong, Long-wavelength-absorbing dialkylphenacylsulfonium salt photoinitiators: Synthesis and photoinduced cationic polymerization, J. Polym. Sci. A Polym. Chem. 38 (2000) 1433–1442. [https://doi.org/10.1002/\(SICI\)1099-0518\(20000501\)38:9<1433::AID-POLA5>3.0.CO;2-W](https://doi.org/10.1002/(SICI)1099-0518(20000501)38:9<1433::AID-POLA5>3.0.CO;2-W).

[32] N. Zivic, M. Bouzrati-Zerrelli, S. Villotte, F. Morlet-Savary, C. Dietlin, F. Dumur, D. Gigmes, J.P. Fouassier, J. Lalevée, A novel naphthalimide scaffold based iodonium salt as a one-component photoacid/photoinitiator for cationic and radical polymerization under LED exposure, Polym. Chem. 7 (2016) 5873–5879. <https://doi.org/10.1039/C6PY01306F>.

[33] G. Hizal, Y. Yağci, W. Schnabel, N-alkoxy pyridinium ion terminated polytetrahydrofurans. Synthesis and their use in photoinitiated block copolymerization, Polymer. 35 (1994) 4443–4448. [https://doi.org/10.1016/0032-3861\(94\)90105-8](https://doi.org/10.1016/0032-3861(94)90105-8).

[34] Y. Yagci, A. Kornowski, W. Schnabel, N-alkoxy-pyridinium and N-alkoxy-quinolinium salts as initiators for cationic photopolymerizations, J. Polym. Sci. A Polym. Chem. 30 (1992) 1987–1991. <https://doi.org/10.1002/pola.1992.080300922>.

[35] L. Atmaca, I. Kayihan, Y. Yagci, Photochemically and thermally induced radical promoted cationic polymerization using allyl phosphonium salts, Polymer. 41 (2000) 6035–6041. [https://doi.org/10.1016/S0032-3861\(99\)00878-2](https://doi.org/10.1016/S0032-3861(99)00878-2).

[36] A. Onen, N. Arsu, Y. Yagci, Photoinitiated polymerization of ethyl cyanoacrylate by phosphonium salts, Angew. Makromol. Chem. 264 (1999) 56–59. [https://doi.org/10.1002/\(SICI\)1522-9505\(19990201\)264:1<56::AID-APMC56>3.0.CO;2-5](https://doi.org/10.1002/(SICI)1522-9505(19990201)264:1<56::AID-APMC56>3.0.CO;2-5).

[37] Y. Matano, T. Shinokura, O. Yoshikawa, H. Imahori, Triaryl(1-pyrenyl)bismuthonium Salts: Efficient Photoinitiators for Cationic Polymerization of Oxiranes and a Vinyl Ether, Org. Lett. 10 (2008) 2167–2170. <https://doi.org/10.1021/ol8005453>.

[38] F. Kasapoglu, A. Onen, N. Bicak, Y. Yagci, Photoinitiated cationic polymerization using a novel phenacyl anilinium salt, Polymer. 43 (2002) 2575–2579. [https://doi.org/10.1016/S0032-3861\(02\)00029-0](https://doi.org/10.1016/S0032-3861(02)00029-0).

- [39] M. Jin, X. Wu, J. Xie, J.P. Malval, D. Wan, One/two-photon-sensitive photoacid generators based on benzene oligomer-containing D- $\pi$ -A-type aryl dialkylsulfonium salts, *RSC Adv.* 5 (2015) 55340–55347. <https://doi.org/10.1039/C5RA11350D>.
- [40] Y. Yağci, I. Reetz, Externally stimulated initiator systems for cationic polymerization, *Progr. Polym. Sci.* 23 (1998) 1485–1538. [https://doi.org/10.1016/S0079-6700\(98\)00010-0](https://doi.org/10.1016/S0079-6700(98)00010-0).
- [41] K. Kaya, J. Kreutzer, Y. Yagci, A Charge- Transfer Complex of Thioxanthonephenacyl Sulfonium Salt as a Visible- Light Photoinitiator for Free Radical and Cationic Polymerizations, *ChemPhotoChem.* 3 (2019) 1187–1192. <https://doi.org/10.1002/cptc.201800217>.
- [42] M. Sangermano, I. Roppolo, A. Chiappone, New Horizons in Cationic Photopolymerization, *Polymers.* 10 (2018) 136. <https://doi.org/10.3390/polym10020136>.
- [43] S. Dadashi-Silab, S. Doran, Y. Yagci, Photoinduced Electron Transfer Reactions for Macromolecular Syntheses, *Chem. Rev.* 116 (2016) 10212–10275. <https://doi.org/10.1021/acs.chemrev.5b00586>.
- [44] J. Crivello, Sensitization of Cationic Photopolymerizations, in: J. Lalevée, J.-P. Fouassier (Eds.), *Dyes and Chromophores in Polymer Science*, John Wiley & Sons, Inc., Hoboken, NJ, USA, 2015: pp. 45–79. <https://doi.org/10.1002/9781119006671.ch2>.
- [45] J.-P. Fouassier, F. Morlet-Savary, J. Lalevée, X. Allonas, C. Ley, Dyes as Photoinitiators or Photosensitizers of Polymerization Reactions, *Materials.* 3 (2010) 5130–5142. <https://doi.org/10.3390/ma3125130>.
- [46] P. Xiao, J. Zhang, F. Dumur, M.A. Tehfe, F. Morlet-Savary, B. Graff, D. Gigmes, J.P. Fouassier, J. Lalevée, Visible light sensitive photoinitiating systems: Recent progress in cationic and radical photopolymerization reactions under soft conditions, *Progr. Polym. Sci.* 41 (2015) 32–66. <https://doi.org/10.1016/j.progpolymsci.2014.09.001>.
- [47] J. Lalevée, F. Dumur, M.-A. Tehfe, A. Zein-Fakih, D. Gigmes, F. Morlet-Savary, B. Graff, J.-P. Fouassier, Dye photosensitized cationic ring-opening polymerization: Search for new dye skeletons, *Polymer.* 53 (2012) 4947–4954. <https://doi.org/10.1016/j.polymer.2012.08.067>.
- [48] P. Sautrot-Ba, S. Jockusch, J.-P. Malval, V. Brezová, M. Rivard, S. Abbad-Andaloussi, A. Blacha-Grzechnik, D.-L. Versace, Quinizarin Derivatives as Photoinitiators for Free-Radical and Cationic Photopolymerizations in the Visible Spectral Range, *Macromolecules.* 53 (2020) 1129–1141. <https://doi.org/10.1021/acs.macromol.9b02448>.
- [49] M. Condat, J. Babinot, S. Tomane, J.-P. Malval, I.-K. Kang, F. Spillebout, P.-E. Mazeran, J. Lalevée, S.A. Andalloussi, D.-L. Versace, Development of photoactivable



glycerol-based coatings containing quercetin for antibacterial applications, *RSC Adv.* 6 (2016) 18235–18245. <https://doi.org/10.1039/C5RA25267A>.

[50] S. Van Schoubroeck, M. Van Dael, S. Van Passel, R. Malina, A review of sustainability indicators for biobased chemicals, *Renew. Sustainable Energy Rev.* 94 (2018) 115–126. <https://doi.org/10.1016/j.rser.2018.06.007>.

[51] X.S. Sun, Overview of Plant Polymers, in: *Handbook of Biopolymers and Biodegradable Plastics*, Elsevier, 2013: pp. 1–10. <https://doi.org/10.1016/B978-1-4557-2834-3.00001-X>.

[52] B. Lochab, I.K. Varma, J. Bijwea, Sustainable Polymers Derived From Naturally Occurring Materials, *AMPC.* 02 (2012) 221–225. <https://doi.org/10.4236/ampc.2012.24B056>.

[53] B. Lochab, S. Shukla, I.K. Varma, Naturally occurring phenolic sources: monomers and polymers, *RSC Adv.* 4 (2014) 21712–21752. <https://doi.org/10.1039/C4RA00181H>.

[54] J.C. O'Connor, R.E. Chapin, Critical evaluation of observed adverse effects of endocrine active substances on reproduction and development, the immune system, and the nervous system, *Pure Appl. Chem.* 75 (2003) 2099–2123. <https://doi.org/10.1351/pac200375112099>.

[55] H. Okada, T. Tokunaga, X. Liu, S. Takayanagi, A. Matsushima, Y. Shimohigashi, Direct Evidence Revealing Structural Elements Essential for the High Binding Ability of Bisphenol A to Human Estrogen-Related Receptor- $\gamma$ , *Environ. Health Perspect.* 116 (2008) 32–38. <https://doi.org/10.1289/ehp.10587>.

[56] F.S. Vom Saal, Bisphenol A and Risk of Metabolic Disorders, *JAMA.* 300 (2008) 1353. <https://doi.org/10.1001/jama.300.11.1353>.

[57] S. Molina- Gutiérrez, A. Manseri, V. Ladmiral, R. Bongiovanni, S. Caillol, P. Lacroix- Desmazes, Eugenol: A Promising Building Block for Synthesis of Radically Polymerizable Monomers, *Macromol. Chem. Phys.* 220 (2019) 1900179. <https://doi.org/10.1002/macp.201900179>.

[58] S. Stoll, A. Schweiger, EasySpin, a comprehensive software package for spectral simulation and analysis in EPR, *J. Magn. Reson.* 178 (2006) 42–55. <https://doi.org/10.1016/j.jmr.2005.08.013>.

[59] C. Lorenzini, A. Haider, I.-K. Kang, M. Sangermano, S. Abbad-Andalloussi, P.-E. Mazeran, J. Lalevée, E. Renard, V. Langlois, D.-L. Versace, Photoinduced Development of Antibacterial Materials Derived from Isosorbide Moiety, *Biomacromolecules.* 16 (2015) 683–694. <https://doi.org/10.1021/bm501755r>.

[60] T. Modjinou, D.-L. Versace, S. Abbad-Andaloussi, V. Langlois, E. Renard, Antibacterial and antioxidant photoinitiated epoxy co-networks of resorcinol and eugenol derivatives, *Mater. Today Commun.* 12 (2017) 19–28. <https://doi.org/10.1016/j.mtcomm.2017.03.005>.

- [61] A. Carocci, A. Catalano, F. Corbo, A. Duranti, R. Amoroso, C. Franchini, G. Lentini, V. Tortorella, Stereospecific synthesis of mexiletine and related compounds: Mitsunobu versus Williamson reaction, *Tetrahedron: Asymmetry*. 11 (2000) 3619–3634. [https://doi.org/10.1016/S0957-4166\(00\)00332-3](https://doi.org/10.1016/S0957-4166(00)00332-3).
- [62] C. Elia, V. Brezová, P. Sautrot-Ba, M. Breza, D.-L. Versace, Lawsons Derivatives as Efficient Photopolymerizable Initiators for Free-Radical, Cationic Photopolymerizations, and Thiol—Ene Reactions, *Polymers*. 13 (2021) 2015. <https://doi.org/10.3390/polym13122015>.
- [63] M. Neda, K. Okinaga, M. Shibata, High-performance bio-based thermosetting resins based on bismaleimide and allyl-etherified eugenol derivatives, *Mater. Chem. Phys.* 148 (2014) 319–327. <https://doi.org/10.1016/j.matchemphys.2014.07.050>.
- [64] M. Leemhuis, N. Akeroyd, J.A.W. Kruijtz, C.F. van Nostrum, W.E. Hennink, Synthesis and characterization of allyl functionalized poly( $\alpha$ -hydroxy)acids and their further dihydroxylation and epoxidation, *Eur. Polym. J.* 44 (2008) 308–317. <https://doi.org/10.1016/j.eurpolymj.2007.12.004>.
- [65] H. Görner, Photoreduction of 9,10-Anthraquinone Derivatives: Transient Spectroscopy and Effects of Alcohols and Amines on Reactivity in Solution, *Photochem. Photobiol.* 77 (2007) 171–179. [https://doi.org/10.1562/0031-8655\(2003\)0770171POADTS2.0.CO2](https://doi.org/10.1562/0031-8655(2003)0770171POADTS2.0.CO2).
- [66] L. Breloy, R. Losantos, D. Sampedro, M. Marazzi, J.-P. Malval, Y. Heo, J. Akimoto, Y. Ito, V. Brezová, D.-L. Versace, Allyl amino-thioxanthone derivatives as highly efficient visible light H-donors and co-polymerizable photoinitiators, *Polym. Chem.* 11 (2020) 4297–4312. <https://doi.org/10.1039/D0PY00551G>.
- [67] K.W. Krosley, G.J. Gleicher, Radical reactions of epoxides. 2. intramolecular competition between cyclopropylmethyl and oxiranylmethyl radical ring-opening rearrangements, *J. Phys. Org. Chem.* 6 (1993) 228–232. <https://doi.org/10.1002/poc.610060406>.
- [68] J. Amaudrut, O. Wiest, Epoxide Formation by Ring Closure of the Cinnamyloxy Radical, *Org. Lett.* 2 (2000) 1251–1254. <https://doi.org/10.1021/ol005749t>.

## Table of Contents

